Received: 17 February 2023 | Accepted: 8 May 2023

DOI: 10.1002/agg2.20392

Agrosystems, Geosciences & Environment OPEN ACCESS

ORIGINAL ARTICLE

Agrosystems

Estimating fall-harvested alfalfa (*Medicago sativa* L.) yield using unmanned aerial vehicle–based multispectral and thermal images in southern California

Anish Sapkota[1,2] | **Amir Haghverdi**[1] | **Ali Montazar**[3]

[1]Department of Environmental Sciences, University of California, Riverside, California, USA

[2]Department of Land, Air and Water Resources, University of California, Davis, California, USA

[3]Division of Agriculture and Natural Resources, UC Cooperative Extension Imperial County, University of California, Holtville, California, USA

Correspondence
Anish Sapkota and Amir Haghverdi, Department of Environmental Sciences, University of California, Riverside, CA, USA.
Email: asapk001@ucr.edu; amirh@ucr.edu

Assigned to Associate Editor Waltram Ravelombola.

Funding information
USDA-NIFA, Grant/Award Number: 2019-68017-29693

Abstract

This study aims to evaluate the efficacy of simple linear, multiple, and robust regression methods to predict fall-harvested alfalfa (*Medicago sativa* L.) yield using unmanned aerial vehicle (UAV)-acquired multispectral and thermal images. Four alfalfa fields in southern California were selected, and a composite dataset containing 180 ground truth sampling points was formed to build and test the performance of the regression models. The UAV was flown in September 2020, 5–29 days before the ground truth data collection. A total of nine crop indices, canopy temperature, and the difference between canopy temperature and air temperature were used as input predictors. Among the simple linear models, the model with normalized difference vegetation index as input showed a strong performance (coefficient of determination [R^2] = 0.76; root mean square error [RMSE] = 170.29 kg ha^{-1}; and mean absolute error [MAE] = 132.18 kg ha^{-1}). A multiple linear regression model with three input predictors showed the highest accuracy with R^2 = 0.83, RMSE = 142.99 kg ha^{-1}, and MAE = 109.30 kg ha^{-1}. The top-performing models accurately estimated mean yield at the field level and differentiated fields with low and high alfalfa productivity. Including canopy temperature-related inputs did not improve the yield prediction power of the models. The error in the yield prediction increased as the days between UAV flights and field harvest increased. Results here suggested that UAV-based remote sensing has the potential to estimate fall-harvested alfalfa yield in southern California.

Abbreviations: BIC, Bayesian information criterion; CWSI, crop water stress index; EVI, enhance vegetation index; GNDVI, green normalized difference vegetation index; LM, linear model; MAE, mean absolute error; MLR, multiple linear regression; NDVI, normalized difference vegetation index; OSAVI, optimized soil adjusted vegetation index; PSRI, plant senescence reflectance index; RMSE, root mean square error; RR, robust regression; RVI, ratio vegetation index; SAVI, soil adjusted vegetation index; SIPI, structure insensitive pigment index; UAV, unmanned aerial vehicle.

1 | INTRODUCTION

Predicting crop yield before harvest is important to make an informed decision on import and export, evaluate the national food security status, and develop profitable market plans (Horie et al., 1992). Crop producers would also be able to apply site-specific variable rates of agricultural inputs if they could know the within and between fields yield variability (Haghverdi et al., 2015; Penney et al., 1996). Additionally, rapid and timely yield estimations can help inform planning of harvest relative to farm labor, equipment, crop market demands, and environmental conditions.

Alfalfa (*Medicago sativa* L.) is a major perennial forage crop well-known for its high dry matter yield, nutritional quality, and palatability (Higginbotham et al., 2008; Sapkota et al., 2019). In the United States, it was the fourth most widely grown crop with an approximate production of 50 million Mg of alfalfa and alfalfa mixtures from over 6.8 million ha of harvested area in 2019 (USDA-NASS, 2020). California leads the nation in alfalfa hay production (CDFA, 2020). Dairy cattle are a significant consumer of alfalfa hay, accounting for up to 75–80% of total utilization (Higginbotham et al., 2008). Since alfalfa is a primary source of feedstock, a decrease in its production rate can be of significant concern. It may even cause forage scarcity for dairy cattle. Therefore, early estimation of alfalfa production can help growers plan for site-specific agricultural management, and investors, consulting agencies, and policymakers prepare beforehand for the import and export of the hay depending upon the yield prediction (Feng et al., 2020).

Destructive sampling and plant maturity assessment are traditional ways of estimating alfalfa yield (Noland et al., 2018). Nevertheless, these methods are demanding, time consuming (Feng et al., 2020; Noland et al., 2018), and may not be accurate for large fields with spatial heterogeneity. An alternative new approach for yield estimation is remote sensing via unmanned aerial vehicles (UAVs), which is gaining popularity because of its ease of use and potential for rapid measurements from the field to the regional scale. UAV-mounted multispectral cameras can be used to obtain a wide range of vegetation indices to evaluate vegetation cover, growth, and vigor and estimate crop yield (Xue & Su, 2017). In addition, UAV-mounted thermal cameras can be used to derive indices like crop water stress index (CWSI) and the difference between canopy temperature and air temperature to detect water stress and estimate crop yield (Chandel et al., 2021; Hattendorf et al., 1988; Kirkham et al., 1983; Zhang et al., 2019). Therefore, selecting an appropriate vegetation index is vital in crop yield estimation.

Estimation of crop yield using remotely sensed images from UAVs and various satellite products has been well studied for cereals crops, including maize (Schwalbert et al., 2018), wheat (Segarra et al., 2020; Zhang et al., 2020), and rice (Arumugam et al., 2021; Fernandez-Beltran et al., 2021; Huang et al., 2013). In addition, several recent studies have also used satellite or UAV-acquired remote sensing images to develop alfalfa yield predicting models and reported promising results (Chandel et al., 2021; Dvorak et al., 2021; Feng et al., 2020). However, UAV-based yield prediction methods are region specific and are affected by various factors, including landscapes, soil quality, and climatic conditions (Rashid et al., 2021; Schwalbert et al., 2018), and no study has investigated both within- and between-field alfalfa yield variability using UAV-acquired multispectral and thermal images. Furthermore, information on the impact of the time difference between UAV flights and alfalfa field harvest on the performance of statistical models is lacking in the literature. Therefore, this study was conducted in the southern California desert agricultural region to estimate the efficacy of UAV-based multispectral and thermal imageries taken close to or well ahead of the harvest for in-season alfalfa yield estimation. The specific objective was to assess the performance of crop indices and accuracy of statistical models to predict yield from fall-harvested alfalfa.

Core Ideas

- Yield predicting models developed here helped to distinguish between-field variability.
- Multiple linear models showed better yield predicting power than simple linear model.
- Among linear models, NDVI-based model predicted fall-harvested alfalfa dry matter yield with greater accuracy.

2 | MATERIALS AND METHODS

2.1 | Study area

This study was conducted in four different commercial alfalfa fields located in the Palo Verde region of southern California (Figure 1). The minimum mean daily temperature for 2020 was approximately 6°C while the maximum mean daily temperature recorded was 40°C, with a mean annual temperature of 23°C. Yearly total rainfall and reference evapotranspiration recorded for the year 2020 was 83 and 1888 mm, respectively, as recorded by the California Irrigation Management Information System (CIMIS) weather station at Ripley, CA. The soil texture, organic matter content, and pH information at multiple depths for all four fields are presented in Table 1 (Montazar et al., 2020). The soil texture varied between the

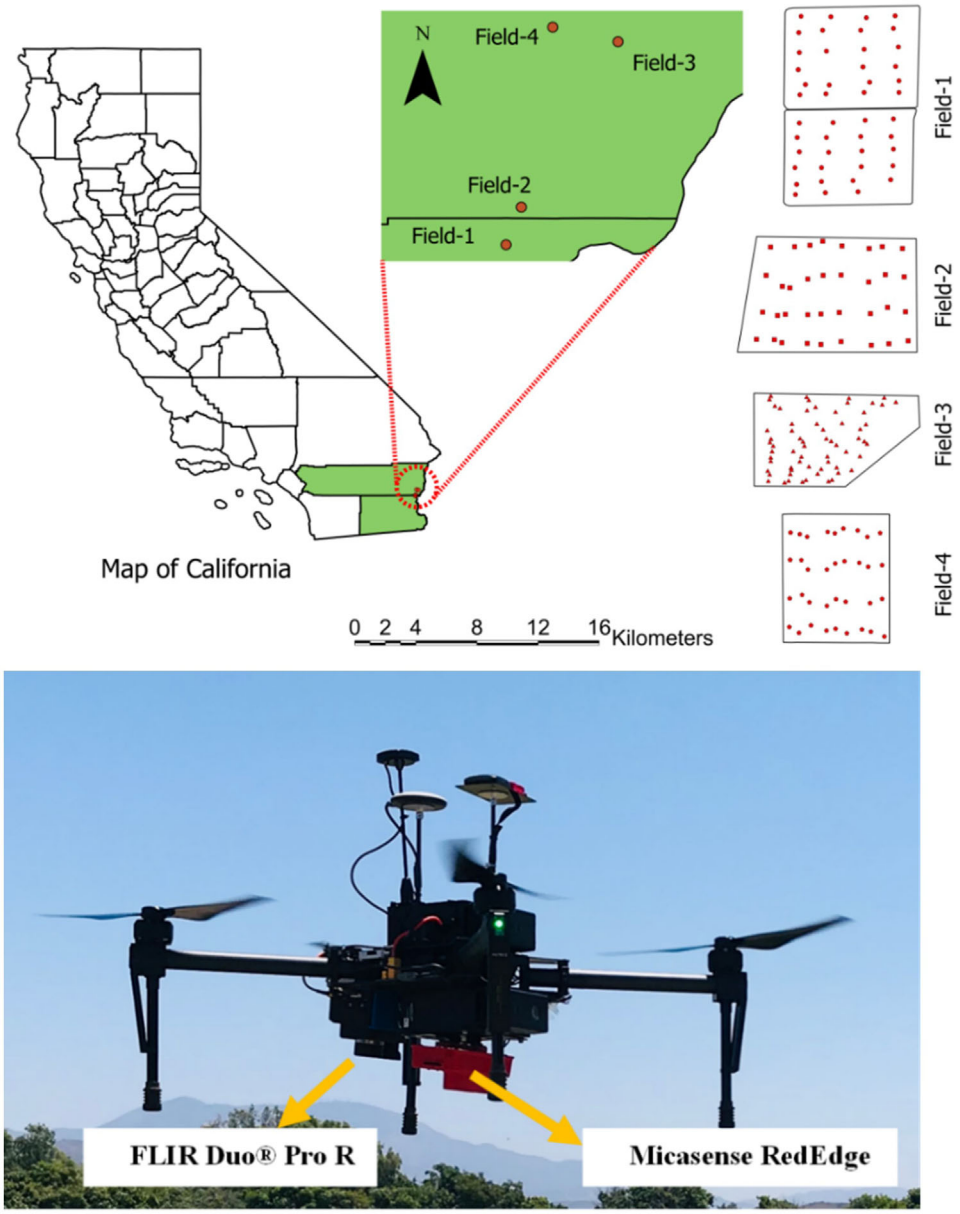

FIGURE 1 At the top, map shows four different study areas and yield sampling points. At the bottom is a picture of DJI Matrice-100 unmanned aerial vehicle (UAV) with the Micasense Rededge and FLIR Duo® Pro R thermal cameras.

study sites. Field-1 mostly had loamy soil. At Field-2, the soil was loamy in the shallow layer (0–0.6 m), while sandy loam (0.6–0.9 m) or loamy sand (0.9–1.2 m) in the deeper layers. Similarly, Field-3 had silt loam soil in the shallow (0–0.6 m) and sandy soil in the deep layers (0.6–1.2 m). Field-4 mostly had sandy soil; however, it was sandy loam in the top-soil layer (0–0.3 m). The soil pH for all the fields was close to 8.0 (7.9–8.4; Table 1).

2.2 | Field data collection

A DJI Matrice 100 quadcopter (SZ DJI Technology Co., Ltd) equipped with Micasense Red Edge multispectral (Micasense, Inc.) and FLIR Duo Pro R thermal (Teledyne FLIR LLC.) cameras (Figure 1) was flown over all four fields on September 26, 2020 on a sunny and cloud-free day ideal for image acquisition. The multispectral camera had five-band sensors, including blue (475 ± 10 nm), green (560 ± 10 nm), red (668 ± 5 nm), red edge (717 ± 5 nm), and near-infrared (840 ± 20 nm). The FLIR Duo Pro R had two lenses, including thermal and visible. The thermal sensor resolution was 336 × 256, and the camera had an accuracy of ±5°C. Images obtained from the cameras were geotagged using the Micasense and FLIR Duo Pro R UAV-mounted GPS sensors. In addition, images of the Micasense standard white reflectance panel were captured before each flight for the radiometric calibration, following the recommended procedure by the

TABLE 1 Soil physiochemical properties of the study fields. Extracted from Montazar et al. (2020).

Experimental site	Horizon (m)	Soil texture			Organic matter (%)	pH
		Sand (%)	Clay (%)	Silt (%)		
Field-1	0–0.3	44.2	11.1	44.7	1.7	8.0
	0.3–0.6	46.9	8.1	45.0	0.8	8.1
	0.6–0.9	41.7	7.7	50.5	0.9	8.2
	0.9–1.2	47.8	5.9	46.3	0.7	8.2
Field-2	0–0.3	39.7	20.6	39.7	2.3	8.1
	0.3–0.6	50.1	11.9	37.9	0.7	8.0
	0.6–0.9	75.0	5.1	19.9	0.9	8.2
	0.9–1.2	83.7	4.1	12.2	0.8	8.2
Field-3	0–0.3	31.5	13.2	55.3	1.3	8.0
	0.3–0.6	26.1	18.7	55.2	0.8	8.1
	0.6–0.9	88.6	2.8	8.6	0.5	8.2
	0.9–1.2	94.8	1.4	3.8	0.5	8.4
Field-4	0–0.3	69.3	13.1	17.6	1.7	7.9
	0.3–0.6	91.9	2.8	5.3	0.8	8.2
	0.6–0.9	82.0	8.3	9.7	1.2	8.1
	0.9–1.2	85.9	5.7	8.4	0.9	8.3

TABLE 2 Dates for unmanned aerial vehicle (UAV) image acquisition, alfalfa harvest (yield sampling), and the time interval between the flight and harvest.

Sites	Date of UAV flight	Date of alfalfa harvest	Days between UAV flight and harvest
Field-1	September 26, 2020	October 1, 2020	5
Field-2	September 26, 2020	October 6, 2020	10
Field-3	September 26, 2020	October 20, 2020	24
Field-4	September 26, 2020	October 25, 2020	29

manufacturer. The mission planning of the flight was configured and implemented in a grid pattern using Pix4Dcapture software (Pix4D S.A.) installed on an iPad mini (Apple Inc.). The flight altitude was approximately 119 m above ground level with the frontal- and side-overlapping of 70%.

Data from a total of 46, 35, 64, and 35 randomly selected sampling plots (1.5 m × 2 m) for fields 1, 2, 3, and 4, respectively, were used in this study. Hand harvesting of all fields was done right before the growers harvested their fields and within 1 month after the UAV data collection (Table 2) and their locations were recorded using Trimble R2 GNSS GPS sensor (Trimble Inc.). Plants were cut at 6–8 cm height, and their fresh weights were recorded. Then, samples were transported to the laboratory and dried for 3 days in a conventional oven at 60°C to obtain alfalfa dry matter weight for each sampling plot. These fields were part of ongoing on-farm irrigation research trials. Each field had been divided into three large plots that received a different irrigation treatment ranging from typical irrigation management by the growers to multiple summer-deficit irrigation strategies. Montazar et al. (2020) outlined more information regarding the irrigation trials.

2.3 | UAV image processing, model development, and implementation

The UAV-acquired images were imported to the photogrammetry software Pix4Dmapper (Version 4.6.4, Pix4D S.A.) for further processing (Figure 2). First, orthomosaic of radiometrically calibrated images were created using multispectral (blue, green, red, red edge, and near-infrared) and thermal cameras for each field. Then, a total of nine indices, including normalized difference vegetation index (NDVI; Rouse et al., 1973), enhanced vegetation index (EVI; Huete et al., 2002), green normalized difference vegetation index (GNDVI; Gitelson et al., 1996), optimized soil adjusted vegetation index (OSAVI; Rondeaux et al., 1996), plant senescence reflectance

TABLE 3 Vegetation indices used in the study and their respective computation methods.

Vegetation index	Equation[a]	Reference
Normalized difference vegetation index (NDVI)	$NDVI = \frac{NIR-RED}{NIR+RED}$	(Rouse et al., 1973)
Enhance vegetation index (EVI)	$EVI = \frac{2.5*(NIR-RED)}{NIR+6*RED-7.5*BLUE+1}$	(Huete et al., 2002)
Green normalized difference vegetation index (GNDVI)	$GNDVI = \frac{NIR-GREEN}{NIR+GREEN}$	(Gitelson et al., 1996)
Optimized soil adjusted vegetation index (OSAVI)	$OSAVI = \frac{NIR-RED}{NIR+RED+0.16}$	(Rondeaux et al., 1996)
Plant senescence reflectance index (PSRI)	$PSRI = \frac{RED-GREEN}{NIR}$	(Merzlyak et al., 1999)
Ratio vegetation index (RVI)	$RVI = \frac{NIR}{RED}$	(Major et al., 1990)
Soil adjusted vegetation index (SAVI)	$SAVI = \frac{NIR-RED}{(NIR+RED+0.5)}*1.5$	(Huete, 1988)
Structure insensitive pigment index (SIPI)	$SIPI = \frac{NIR-BLUE}{NIR-RED}$	(Penuelas et al., 1995)
Crop water stress index (CWSI)	$CWSI = \frac{((T_{canopy}-T_{air})_M-(T_{canopy}-T_{air})_L)}{((T_{canopy}-T_{air})_U-(T_{canopy}-T_{air})_L)}$	(Jackson et al., 1981)

Abbreviations: L, lower baseline; *M*, measured; NIR, near infrared; T_{air}, air temperature (C°); T_{canopy}, canopy temperature (C°); U, upper baseline.

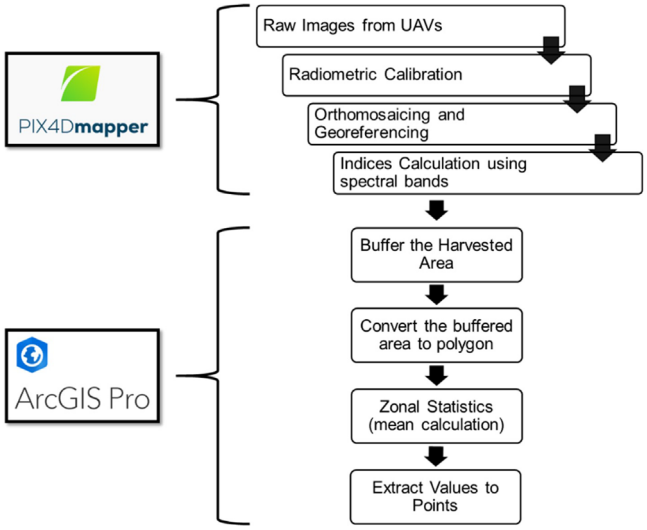

FIGURE 2 Flowchart shows the workflow of unmanned aerial vehicle (UAV) image processing using the PIX4Dmapper and ArcGIS Pro software packages.

index (PSRI; Major et al., 1990; Merzlyak et al., 1999), ratio vegetation index (RVI; Major et al., 1990), soil adjusted vegetation index (SAVI; Huete, 1988), structure insensitive pigment index (SIPI; Penuelas et al., 1995), thermal images representing canopy temperature, and CWSI, were computed. Raster images for canopy temperature were obtained only for Field-2, -3, and -4. Table 3 summarizes the band combinations for all the vegetation indices used in this study. The CWSI was computed for three fields (Field-2, -3, and -4) using field specific baselines (CWSI-F) and overall baselines for the composite dataset (CWSI-C). In other words, the CWSI-F was calculated for each field using the minimum and maximum canopy temperature of that particular field, while the minimum and maximum canopy temperature of the composite dataset was used to calculate the CWSI-C for all the fields.

Raster images for each vegetation index and thermal image created in Pix4Dmapper (Pix4D S.A.) were imported to ArcGIS Pro 2.8 (ESRI Inc.) for the feature extraction and further analysis (Figure 2). First, geo-coordinates of the ground sampling locations from where the alfalfa was hand-harvested were used to pin the locations in each raster image. A polygon of size 1.5–1.8 m^2 was created around all the geo-coordinates to extract the mean values of different vegetation indices. Then, a raster calculator was used to compute the mean values for each point feature.

Figure 3 shows the steps involved in developing and validating the yield predicting models. The actual yield data and information extracted from the raster image of the vegetation indices for all four fields were merged to make a composite dataset. Therefore, the yield collected from a total of 180 sampling locations ($n = 134$ from Field-2, -3, and -4 for models involving thermal data) was considered during the model development process. A total of 10 models were developed in this study using simple, multiple, and robust regression techniques. Ten simple linear regression models (with one input predictor) were created using the eight vegetation indices, including NDVI, EVI, GNDVI, OSAVI, PSRI, RVI, SAVI, and SIPI, canopy temperature, and canopy minus air temperature (dT). The mean air temperature values for the flight duration for each field were obtained from the closest CIMIS weather station.

The "leaps" package in RStudio (Lumley & Miller, 2020) was used to select the most important crop indices for multiple regression models through the branch-and-bound algorithm (Lumley & Miller, 2020). Then, the Bayesian information

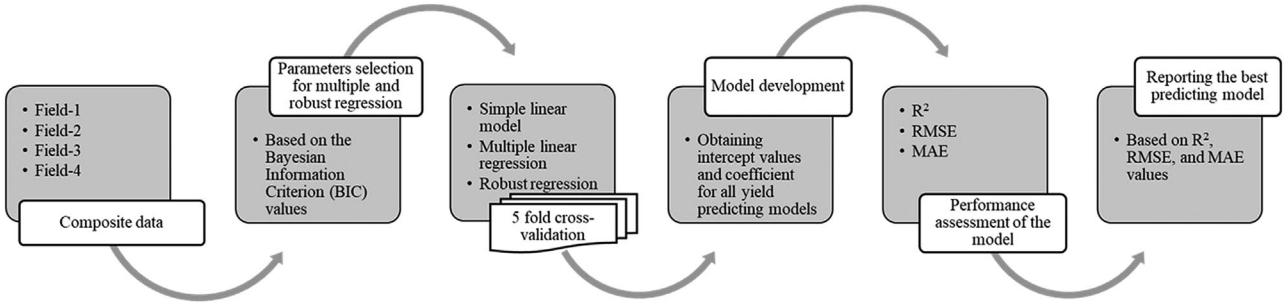

FIGURE 3 Flow diagram showing the process of model development and model selection.

criterion (BIC) was used to determine the best representative subset of the crop indices. Similarly, this process was repeated to evaluate the prediction power of the models when we included thermal data from three fields in addition to the multispectral images. A robust regression model was also developed using the same subset of predictor variables as multiple regression models. Since the data used in this study are from multiple fields with varying irrigation rates and soil types, the robust regression model was developed to accommodate all data points rather than treating extreme values as outliers "Robust regression" (n.d). The composite dataset was randomly divided into five equal size folds. Four folds were used to develop the models, and the remaining fold was utilized to test their accuracy. This process was repeated five times, and each time a different fold was used as the test subset.

The best-performing models were used to predict the total alfalfa yield at each field. Raster images of all the needed vegetation indices were converted to 2 m × 2 m resolution. Next, the NDVI maps were converted from raster to points for each field, and any NDVI values less than 0.2 were removed as they represent nonvegetation or bare soil surface (Montandon & Small, 2008). Then, the filtered NDVI images were used to mask raster images of other vegetation indices. Once the masking was done, all raster images obtained using multispectral bands were converted to point features. In total, 25,185, 30,286, 41,316, and 26,182 data points (pixel counts) were extracted for each vegetation indices from the Field-1, Field-2, Field-3, and Field-4, respectively. For each data point, alfalfa yield was predicted using the best-performing models, and the mean yield for each field was determined.

2.4 | Model evaluation

The performance of the models was evaluated using the coefficient of determination (R^2; Equation 1), the root mean square error (RMSE; Equation 2), and the mean absolute error (MAE; Equation 3) for the composite dataset and separately for individual fields.

$$R^2 = 1 - \frac{\sum_{i=1}^{N}(M_i - E_i)^2}{\sum_{i=1}^{N}(M_i - \bar{M})^2} \quad (1)$$

$$\text{RMSE} = \sqrt{\frac{1}{N}\sum_{i=1}^{N}(E_i - M_i)^2} \quad (2)$$

$$\text{MAE} = \frac{1}{N}\sum_{i=1}^{N}|E_i - M_i| \quad (3)$$

where N is the total number of observations, M_i is the measured and E_i is the predicted value of ith observation, and $\bar{M}$ is the mean of the measured yield values.

3 | RESULTS AND DISCUSSION

3.1 | Variation in actual yield values and vegetation indices across the fields

Table 4 shows the descriptive statistics (minimum, maximum, mean, and standard deviation) of alfalfa dry matter yield and eight different vegetation indices and canopy temperature (thermal) obtained at the sampling locations of four fields. The yield values ranged from 1952 to 2726 kg ha^{-1}, with Field-2 and Field-3 having the maximum and minimum dry matter yield, respectively. The yield data used for this study are associated with the September harvest cycle for Field-1 and Field-2 and the October harvest cycle for Field-3 and Field-4. Alfalfa dry matter yields are typically higher during the September harvest cycle than in the October harvest cycle in the region, partly explaining the relatively higher yields at Field-1 and Field-2. In addition, all four fields were exposed to different irrigation levels and had different soil types, which

TABLE 4 Distribution of actual alfalfa dry matter yield and the vegetation indices and canopy temperature data at the four fields used in this study.

Experiemental site	Yield (kg ha^{-1})	NDVI	EVI	GNDVI	OSAVI	PSRI	RVI	SAVI	SIPI	Thermal (˚C)
Field-1 (Harvested 5 days after the UAV flight)										
Minimum	2219.28	0.92	0.22	−0.83	0.36	−0.08	24.52	0.23	0.97	–
Maximum	2712.46	0.94	0.32	−0.80	0.45	−0.06	33.15	0.33	0.99	–
Mean	2573.57	0.93	0.25	−0.81	0.39	−0.07	28.68	0.27	0.98	–
SD	91.43	0.005	0.02	0.01	0.02	0.004	2.09	0.02	0.003	–
Field-2 (Harvested 10 days after the UAV flight)										
Minimum	2421.04	0.78	0.05	−0.72	0.11	−0.14	11.62	0.06	0.94	20.59
Maximum	2959.04	0.93	0.08	−0.64	0.16	−0.09	26.81	0.09	0.97	32.27
Mean	2726.55	0.90	0.07	−0.70	0.14	−0.12	21.60	0.08	0.95	26.27
SD	121.14	0.03	0.01	0.02	0.01	0.01	3.82	0.01	0.005	2.04
Field-3 (Harvested 24 days after the UAV flight)										
Minimum	1658.86	0.32	0.02	−0.46	0.04	−0.18	1.99	0.02	0.87	27.88
Maximum	2443.45	0.65	0.03	−0.26	0.07	−0.06	4.94	0.04	1.06	47.26
Mean	1952.03	0.49	0.02	−0.37	0.05	−0.12	3.20	0.03	0.93	39.16
SD	134.64	0.07	0.003	0.04	0.01	0.03	0.65	0.004	0.04	4.62
Field-4 (Harvested 29 days after the UAV flight)										
Minimum	1726.11	0.56	0.02	−0.61	0.06	−0.20	2.94	0.03	0.37	15.43
Maximum	2802.13	0.88	0.06	−0.33	0.14	−0.13	12.78	0.06	0.72	32.04
Mean	2327.27	0.81	0.04	−0.53	0.11	−0.17	8.66	0.05	0.63	23.00
SD	219.56	0.08	0.01	0.07	0.02	0.01	2.84	0.01	0.09	4.05

Abbreviations: EVI, enhanced vegetation index; GNDVI, green normalized difference vegetation index; NDVI, normalized difference vegetation index; OSAVI, optimized soil adjusted vegetation index; PSRI, plant senescence reflectance index; RVI, relative vigor index; SAVI, soil adjusted vegetation index; SD, standard deviation; SIPI, structure insensitive pigment index.

also contributed to the yield variability between the fields. Between four fields, the alfalfa dry matter yield deviated less from the mean yield at Field-1 (91.43 kg ha^{-1}) and Field-2 (121.14 kg ha^{-1}) than at Field-3 (134.64 kg ha^{-1}) and Field-4 (219.56 kg ha^{-1}). In addition to the variation in the yield, the mean NDVI values at the sampling locations at Field-1 and Field-2 were more than 0.9, while it was only 0.49 and 0.81 in Field-3 and Field-4, respectively. Similarly, other vegetation indices, including EVI, OSAVI, RVI, SAVI, and SIPI, also showed greater absolute values at Field-1 and Field-2 (which were near-ready to get harvested) than at Field-3 and Field-4. The mean canopy temperature at Field-2 and Field-4 was 26 ± 2˚C and 23 ± 4˚C, respectively, while the canopy temperature observed at Field-3 was relatively higher with a mean value of 39 ± 2˚C (Table 4). Overall, Field-2 and Field-4 with lower canopy temperatures had higher yields than Field-3 with higher canopy temperature values.

3.2 | Overall performance of the models for the composite dataset

Table 5 summarizes the performance statistics values for all models developed in this study for the composite dataset and provides the regression equations for all the models. Figure 4 shows the scatter plots of actual versus estimated alfalfa dry matter yield for the top-performing models. Significant relationships were observed between actual and estimated alfalfa dry matter yield for all simple linear models except for LM_{SIPI} (where LM is linear model). Among the simple linear models, LM_{NDVI} showed the best performance (R^2 = 0.76, RMSE = 170.29 kg ha^{-1}, and MAE = 132.18 kg ha^{-1}; Table 5) followed by LM_{GNDVI} (R^2 = 0.74, RMSE = 179.41 kg ha^{-1}, and MAE = 146.69 kg ha^{-1}; Table 5) and LM_{RVI} (R^2 = 0.66, RMSE = 199.90 kg ha^{-1}, and MAE = 158.10 kg ha^{-1}; Table 5). The fit of all other simple linear models that used EVI, OSAVI, PSRI, SAVI, SIPI, canopy temperature, dT, and CWSI as input variables were weak, with a coefficient of determination (R^2) less than 0.54 (Table 5).

Our results are in line with the findings from a study done in Saudi Arabia where the predicted yield using NDVI values from Landsat-8 satellite images had a strong correlation (R^2 = 0.63) with the actual alfalfa yield values (Kayad et al., 2016). Similarly, in an alfalfa study done at Ardmore, OK, Cazenave et al. (2019) estimated alfalfa dry matter yield using UAV-based NDVI and ground coverage data. They also found a strong correlation (R^2 = 0.87) between the harvested

TABLE 5 Different yield prediction models and their performance for the composite dataset.

Models	Regression equations	RMSE (kg ha^{-1})	R^2	MAE (kg ha^{-1})
LM_{NDVI}	Yield (kg ha^{-1}) = 1231.78 + 1479.32 * NDVI	170.29 ± 17.38	0.76 ± 0.05	132.18 ± 9.61
LM_{EVI}	Yield (kg ha^{-1}) = 2150.51 + 1961.19 * EVI	288.53 ± 31.84	0.31 ± 0.11	235.40 ± 31.73
LM_{GNDVI}	Yield (kg ha^{-1}) = 1437.32 − 1559.44 * GNDVI	179.41 ± 28.62	0.74 ± 0.06	146.69 ± 24.31
LM_{OSAVI}	Yield (kg ha^{-1}) = 2082.28 + 1505.40 * OSAVI	273.96 ± 14.08	0.37 ± 0.04	221.83 ± 8.03
LM_{PSRI}	Yield (kg ha^{-1}) = 2535.84 + 1707.47 * PSRI	336.19 ± 19.13	0.04 ± 0.03	294.64 ± 15.41
LM_{RVI}	Yield (kg ha^{-1}) = 1967.94 + 25.54 * RVI	199.90 ± 14.37	0.66 ± 0.07	158.10 ± 10.99
LM_{SAVI}	Yield (kg ha^{-1}) = 2137.59 + 1933.15 * SAVI	285.83 ± 3.22	0.31 ± 0.06	231.77 ± 8.99
LM_{SIPI}	Yield (kg ha^{-1}) = 2062.10 + 306.80 * SIPI	341.14 ± 13.16	0.02 ± 0.02	303.92 ± 12.48
$LM_{Thermal}$	[a]Yield (kg ha^{-1}) = 3142.56 − 28.20 * Thermal	272.11 ± 31.68	0.45 ± 0.10	216.74 ± 21.16
LM_{CWSI-F}	[a]Yield (kg ha^{-1}) = 2742.80 − 1431.00 * CWSI-F	303.77 ± 26.98	0.30 ± 0.05	247.03 ± 29.23
LM_{CWSI-C}	[a]Yield (kg ha^{-1}) = 2765.86 − 1374.84 * CWSI-C	272.11 ± 31.68	0.45 ± 0.10	216.74 ± 21.16
LM_{dT}	[a]Yield (kg ha^{-1}) = 2056.90 − 32.95 * dT	250.27 ± 32.52	0.54 ± 0.08	196.86 ± 23.08
MLR	Yield (kg ha^{-1}) = 1467.00 + 2249.00 * NDVI − 1717.00 * OSAVI + 4419.00 * PSRI	142.99 ± 23.06	0.83 ± 0.04	109.30 ± 14.71
RR	Yield (kg ha^{-1}) = 1473.61 + 2244.35 * NDVI − 1710.96 * OSAVI + 4411.37 * PSRI	143.05 ± 17.41	0.83 ± 0.03	108.65 ± 12.41

Abbreviations: CWSI-C, crop water stress index calculated for all the fields using the minimum and maximum canopy temperature of the composite dataset; CWSI-F, crop water stress index calculated for each field using the minimum and maximum canopy temperature of that particular field; dT, difference of canopy and air temperature in degree Celsius; EVI, enhanced vegetation index; GNDVI, green normalized difference vegetation index; LM, linear models; MAE, mean absolute error; MLR, multiple linear regression; NDVI, normalized difference vegetation index; OSAVI, optimized soil adjusted vegetation index; PSRI, plant senescence reflectance index; R^2, coefficient of determination; RMSE, root mean square error; RR, robust regression; RVI, relative vigor index; SAVI, soil adjusted vegetation index; SIPI, structure insensitive pigment index; Thermal, canopy temperature in degree Celsius; ± represents the standard deviation.

[a]Data from only three fields (Field-2, -3, -4) were used to build these two models that use thermal data.

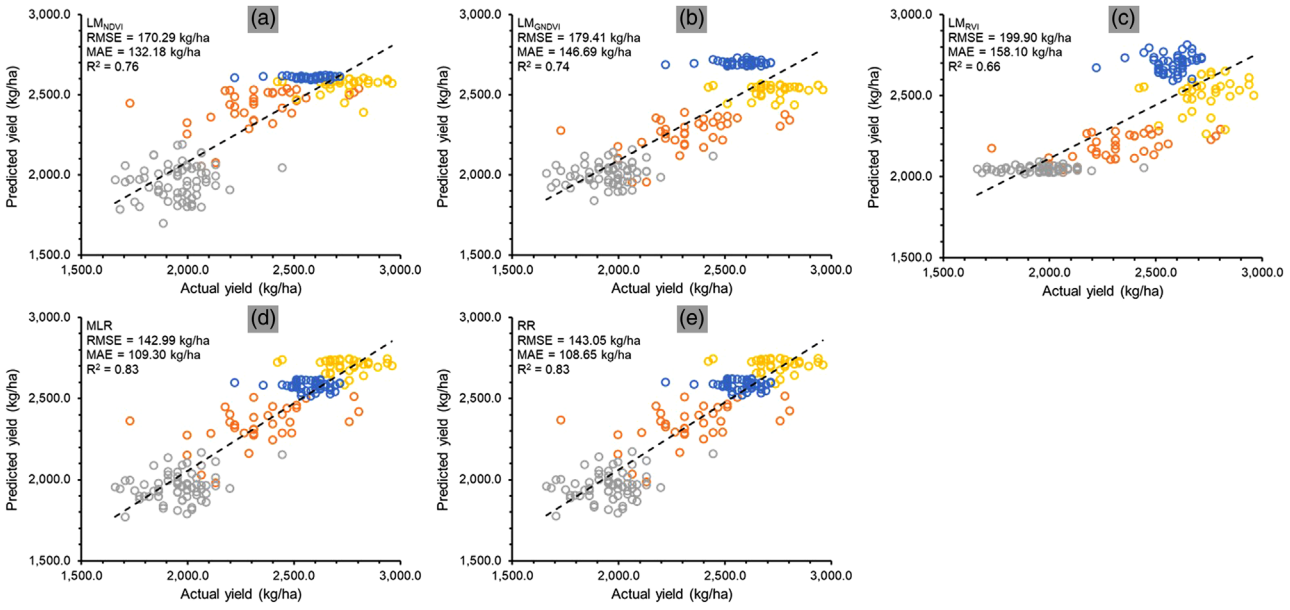

FIGURE 4 Scattered plots showing the relationship between the actual and predicted alfalfa yield for five different models: (a) LM_{NDVI}, (b) LM_{GNDVI}, (c) LM_{RVI}, (d) multiple linear regression (MLR), and (e) robust regression (RR). Colorful rings in the graph represent different fields. Blue = Field-1; yellow = Field-2; gray = Field-3; and orange = Field-4. LM, linear models; RMSE, root mean square error; R^2, coefficient of determination; MAE, mean absolute error; NDVI, normalized difference vegetation index; GNDVI, green normalized difference vegetation index; RVI, relative vigor index.

and estimated dry biomass (Cazenave et al., 2019). However, some contrasting findings suggest NDVI may not be an effective vegetation index to estimate alfalfa yield because of alfalfa's dense canopy that stabilizes the NDVI values with a mean NDVI in the upper spectrum of the scale and ignores within-field variability (Ferencz et al., 2004; Kayad et al., 2016). A recent study at Prosser, WA, also found a weak relation ($R^2 = 0.29$) between NDVI estimated and actual alfalfa yield (Chandel et al., 2021). They indicated that, though NDVI is an effective index at the early crop growth stages, with the vegetative growth and increase in leaf area and plant height, NDVI saturates (Chandel et al., 2021). The high performance of the LM_{NDVI} model in our study is attributed to the (I) high range of NDVI for our composite dataset and (II) expected positive correlation between NDVI and ground vegetation biomass in summer (Borowik et al., 2013).

The GNDVI, which evaluates plant stress by measuring the rates of photosynthesis, is also well used to predict alfalfa yield (Chandel et al., 2021; Noland et al., 2018). Noland et al. (2018) found that their GNDVI-based model made an accurate prediction of alfalfa yield ($R^2 = 0.52$) and forage quality (crude protein; $R^2 = 0.40$). Similarly, Chandel et al. (2021) suggested a positive correlation ($R^2 = 0.43$) between alfalfa yield and GNDVI. These findings are similar to the findings of this study (Model LM_{GNDVI}; Table 5); however, the results obtained in this study suggest a stronger relationship between alfalfa yield and GNDVI ($R^2 = 0.74$; Table 5). On the other hand, the usefulness of the RVI to predict alfalfa yield has not been well studied. However, a positive correlation ($R^2 = 0.66$) between alfalfa yield and LM_{RVI} was observed in this study. Similar findings ($R^2 = 0.89$) between RVI (aka simple ratio) and durum wheat in the Mediterranean region were reported (Royo et al., 2003).

Models developed using multiple linear regression (MLR) and the robust regression (RR) approach showed strong yield predicting abilities (Table 5). The best MLR model included three predictor variables, including NDVI, OSAVI, and PSRI. These three indices were selected based on the BIC values described earlier in Section 2. Canopy temperature and dT were omitted during the parameter selection process, indicating that they were not among the strongest inputs to predict alfalfa yield. However, dT predicted alfalfa yield with better accuracy ($R^2 = 0.54$) than canopy temperature ($R^2 = 0.45$). The MLR fit was significant ($p < 0.001$) to the predicted yield and the relationship was strong ($R^2 = 0.83$, RMSE = 142.99 kg ha^{-1}, and MAE = 109.30 kg ha^{-1}; Table 5). It outperformed all the linear models and compared to the best performing linear model (i.e., LM_{NDVI}) with 7% greater R^2 and 16% lesser RMSE. The RR model also showed equal strength as MLR in predicting alfalfa yield using the same three predictor variables, including NDVI, OSAVI, and PSRI. The fit was significant ($p < 0.001$) and strong ($R^2 = 0.83$, RMSE = 143.05 kg ha^{-1}, and MAE = 108.65 kg ha^{-1}; Table 5). Compared to the best performing linear model (i.e., LM_{NDVI}), the RR model showed a stronger predicting power with 7% greater R^2 and 16% lesser RMSE values.

Of the three predictor variables used in MLR and RR, NDVI measures plant vigor and greenness (Easterday et al., 2019), OSAVI eliminates background soil and estimates aboveground biomass (Xue & Su, 2017), and PSRI measures carotenoid pigment and reflects the canopy stress (Zhang et al., 2018). These predictor variables accounted for the alfalfa's growing condition and physiology, hence resulting in a strong alfalfa yield predicting model. Our finding showed that the canopy temperature related inputs were not as strong candidates for in-season estimation of alfalfa yield. Remote sensing-based statistical yield models are region-specific and may not be suitable for identifying yield variability even at the state level (Schwalbert et al., 2018). Therefore, more research and validation of the models developed in this study are needed to determine whether they can provide reliable alfalfa dry matter yield estimation in other desert agricultural regions worldwide with similar weather conditions.

3.3 | Performance of the models in individual fields

Table 6 summarizes the performance statistics values for the top-performing models for the composite dataset and each individual field. The LM_{NDVI} was the most accurate linear model in Field-1 and Field-2 with RMSE of 98.06 kg ha^{-1} and 203.28 kg ha^{-1}, respectively. The LM_{GNDVI} was the most accurate linear model in Field-3 and Filed-4 with RMSE of 146.58 kg ha^{-1} and 203.08 kg ha^{-1}, respectively. Linear models with canopy temperature or dT did not outperform other models in either of the three fields. The MLR model was the best overall model (RMSE ranging from 98.86 kg ha^{-1} to 193.25 kg ha^{-1}), followed by the RR (RMSE ranging from 99.27 kg ha^{-1} to 193.52 kg ha^{-1}) across all the fields. Consequently, both these models provided the most accurate estimation of mean alfalfa dry matter yield for all fields (Table 7). Field-1 and Field-2 with UAV images collected near the actual field harvest showed lower errors than Field-3 and Field-4, with UAV captured well ahead of the actual field harvest. We attribute this to variations in alfalfa's spectral signature over time across growth stages, which impacts the values of vegetation indices (Shen et al., 2010). Therefore, accurate estimation of alfalfa yields early in the season using UAVs may be challenging, and more studies are needed to evaluate the performance of UAV-based models for yield estimation using images taken at different alfalfa growth stages.

TABLE 6 Performance of the models for composite dataset and individual fields

Models	Composite data	Field-4	Field-3	Field-2	Field-1
Days[a]	R^2	29	24	10	5
LM_{NDVI}	0.76 ± 0.05	0.23	0.02	0.01	0.01
LM_{GNDVI}	0.74 ± 0.06	0.25	0.05	0.01	0.00
LM_{RVI}	0.66 ± 0.07	0.26	0.01	0.02	0.01
MLR	0.83 ± 0.04	0.23	0.07	0.02	0.02
RR	0.83 ± 0.03	0.23	0.07	0.02	0.02
	RMSE (kg ha^{-1})				
LM_{NDVI}	170.29 ± 17.38	215.78	160.60	203.28	98.06
LM_{GNDVI}	179.41 ± 28.62	203.00	146.58	232.01	156.63
LM_{RVI}	199.90 ± 14.37	237.05	165.56	252.09	162.08
MLR	142.99 ± 23.06	193.25	139.67	126.81	98.86
RR	143.05 ± 17.41	193.52	139.96	125.93	99.27
	MAE (kg ha^{-1})				
LM_{NDVI}	132.18 ± 9.61	164.30	132.59	176.92	67.87
LM_{GNDVI}	146.69 ± 24.31	157.48	115.90	210.77	127.69
LM_{RVI}	158.10 ± 10.99	186.89	126.44	220.77	129.68
MLR	109.30 ± 14.71	141.02	115.50	97.11	74.52
RR	108.65 ± 12.41	140.86	115.26	96.01	73.80

Abbreviations: GNDVI, green normalized difference vegetation index; LM, linear models; MAE, mean absolute error; MLR, multiple linear regression; NDVI, normalized difference vegetation index; R^2, coefficient of determination; RMSE, root mean square error; RR, robust regression; RVI, relative vigor index; ± represents the standard deviation.

[a]Days between UAV flight and harvest.

TABLE 7 Mean alfalfa yield obtained using the best performing models for the composite dataset and each field included in the study.

Models	Composite data	Field-1	Field-2	Field-3	Field-4
Days[a]		5	10	24	29
Actual yield, kg ha^{-1} (mean ± SD)	2334.43 ± 342.52	2573.57 ± 92.44	2726.55 ± 122.91	1952.03 ± 135.7	2327.27 ± 222.76
LM_{NDVI}, kg ha^{-1} (mean ± SD)	2334.43 ± 297.67	2583.75 ± 116.09	2573.98 ± 64.36	1941.27 ± 200.02	2387.01 ± 191.64
LM_{GNDVI}, kg ha^{-1} (mean ± SD)	2334.43 ± 291.43	2681.25 ± 86.81	2537.48 ± 56.02	1992.91 ± 113.19	2228.94 ± 161.94
LM_{RVI}, kg ha^{-1} (mean ± SD)	2334.43 ± 278.53	2657.82 ± 165.65	2539.77 ± 122.07	2048.06 ± 30.34	2176.99 ± 91.76
MLR, kg ha^{-1} (mean ± SD)	2334.50 ± 312.24	2575.24 ± 97.96	2705.77 ± 92.03	1948.36 ± 115.71	2317.06 ± 244.43
RR, kg ha^{-1} (mean ± SD)	2339.56 ± 311.83	2580.4 ± 97.72	2710 ± 91.85	1953.92 ± 115.47	2321.92 ± 243.96

Abbreviations: GNDVI, green normalized difference vegetation index; LM, linear models; MLR, multiple linear regression; NDVI, normalized difference vegetation index; RR, robust regression; RVI, relative vigor index; SD, standard deviation.

[a]Days between UAV flight and harvest.

The R^2 values at the field level were substantially lower than the composite dataset. However, the field-level error statistics (RMSE and MAE) were in an acceptable range for all models (Table 6), and they provided an accurate estimation of mean yield for all fields (Table 7). We attribute the low R^2 values to the narrow ranges of vegetation indices and relatively low within-field yield variability for all the fields. The vegetation indices used as input predictors did not detect small yield variabilities in each field. On the other hand, the variation in vegetation indices and yield between the fields was significant. Therefore, models developed using the composite dataset showed promising performance and could detect yield variabilities between the fields, as evident in Figure 4 and high overall R^2 values for the composite dataset.

4 | CONCLUSION

The multiple linear regression model with NDVI, OSAVI, and PSRI as predictor variables (obtained from UAV-based multispectral images) provided the accurate estimation of fall-harvested alfalfa dry matter yield in this study. Including canopy temperature related inputs did not enhance the yield prediction performance of the models. The top UAV-based models in this study distinguished between fields with high and low alfalfa dry matter yield values. The models, however, did not accurately detect within-field yield variabilities, which is attributed to relatively low variability in input predictors and actual yield for each field. Future works are needed to assess the reliability of these fall-harvested yield predicting models in other desert agricultural regions worldwide with similar weather conditions. The potential of satellite-based remote sensing images to estimate the mean alfalfa yield at the field scale can also be assessed. UAV-based remote sensing provides high-resolution data that, if coupled with in-season climatic and crop physio-morphological information, may help build robust yield-predicting models that can identify within-field variability for site-specific precision farming.

AUTHOR CONTRIBUTIONS

Anish Sapkota: Conceptualization; data curation; formal analysis; investigation; methodology; software; validation; visualization; writing—original draft; writing—review and editing. **Amir Haghverdi**: Conceptualization; funding acquisition; methodology; project administration; resources; supervision; validation; writing—review and editing. **Ali Montazar**: Conceptualization; funding acquisition; methodology; project administration; resources; writing—review and editing.

ACKNOWLEDGMENTS

This study was supported by the United States Department of Agriculture–National Institute of Food and Agriculture (USDA NIFA) award 2019-68017-29693. We would also like to acknowledge Jean Claude Iradukunda for his help in the UAV flights.

CONFLICT OF INTEREST STATEMENT

The authors declare no conflicts of interest.

ORCID

Anish Sapkota https://orcid.org/0000-0002-4125-6227
Amir Haghverdi https://orcid.org/0000-0001-5033-6395

REFERENCES

Arumugam, P., Chemura, A., Schauberger, B., & Gornott, C. (2021). Remote sensing based yield estimation of rice (*Oryza sativa* L.) using gradient boosted regression in India. *Remote Sensing*, *13*(12), 2379. https://doi.org/10.3390/rs13122379

Borowik, T., Pettorelli, N., Sönnichsen, L., & Jędrzejewska, B. (2013). Normalized difference vegetation index (NDVI) as a predictor of forage availability for ungulates in forest and field habitats. *European Journal of Wildlife Research*, *59*(5), 675–682. https://doi.org/10.1007/s10344-013-0720-0

Cazenave, A.-B., Shah, K., Trammell, T., Komp, M., Hoffman, J., Motes, C. M., & Monteros, M. J. (2019). High-throughput approaches for phenotyping alfalfa germplasm under abiotic stress in the field. *The Plant Phenome Journal*, *2*(1), 190005. https://doi.org/10.2135/tppj2019.03.0005

CDFA. (2020). *California agricultural statistics review 2019–2020*. California Department of Food and Agriculture. https://www.cdfa.ca.gov/Statistics/PDFs/2020_Ag_Stats_Review.pdf

Chandel, A. K., Khot, L. R., & Yu, L.-X. (2021). Alfalfa (*Medicago sativa* L.) crop vigor and yield characterization using high-resolution aerial multispectral and thermal infrared imaging technique. *Computers and Electronics in Agriculture*, *182*, 105999. https://doi.org/10.1016/j.compag.2021.105999

Dvorak, J. S., Pampolini, L. F., Jackson, J. J., Seyyedhasani, H., Sama, M. P., & Goff, B. (2021). Predicting quality and yield of growing alfalfa from a UAV. *Transactions of the Asabe*, *64*(1), 63–72. https://doi.org/10.13031/trans.13769

Easterday, K., Kislik, C., Dawson, T. E., Hogan, S., & Kelly, M. (2019). Remotely sensed water limitation in vegetation: insights from an experiment with unmanned aerial vehicles (UAVs). *Remote Sensing*, *11*(16), 1853. https://doi.org/10.3390/rs11161853

Feng, L., Zhang, Z., Ma, Y., Du, Q., Williams, P., Drewry, J., & Luck, B. (2020). Alfalfa yield prediction using UAV-based hyperspectral imagery and ensemble learning. *Remote Sensing*, *12*(12), 2028. https://doi.org/10.3390/rs12122028

Ferencz, C., Bognár, P., Lichtenberger, J., Hamar, D., Tarcsai, G., Timár, G., Molnár, G., Pásztor, S. Z., Steinbach, P., Székely, B., Ferencz, O. E., & Ferencz-Árkos, I. (2004). Crop yield estimation by satellite remote sensing. *International Journal of Remote Sensing*, *25*(20), 4113–4149. https://doi.org/10.1080/01431160410001698870

Fernandez-Beltran, R., Baidar, T., Kang, J., & Pla, F. (2021). Rice-yield prediction with multi-temporal Sentinel-2 data and 3D CNN: A case study in Nepal. *Remote Sensing*, *13*(7), 1391. https://doi.org/10.3390/rs13071391

Gitelson, A. A., Kaufman, Y. J., & Merzlyak, M. N. (1996). Use of a green channel in remote sensing of global vegetation from EOS-MODIS. *Remote Sensing of Environment*, *58*(3), 289–298. https://doi.org/10.1016/S0034-4257(96)00072-7

Haghverdi, A., Leib, B. G., Washington-Allen, R. A., Ayers, P. D., & Buschermohle, M. J. (2015). Perspectives on delineating management zones for variable rate irrigation. *Computers and Electronics in Agriculture*, *117*, 154–167. https://doi.org/10.1016/j.compag.2015.06.019

Hattendorf, M. J., Carlson, R. E., Halim, R. A., & Buxton, D. R. (1988). Crop water stress index and yield of water-deficit-stressed alfalfa. *Agronomy Journal*, *80*(6), 871–875. https://doi.org/10.2134/agronj1988.00021962008000060006x

Higginbotham, G. E., Stull, C. L., Peterson, N. G., Rodiek, A. V., Reed, B. A., & Guerrero, J. N. (2008). Alfalfa utilization by livestock. In C. G. Summers & D. H. Putnam (Eds.), *Irrigated alfalfa management in Mediterranean and desert zones* (Publication 8303). University of Califorina Division of Agriculture and Natural Resources.

Horie, T., Yajima, M., & Nakagawa, H. (1992). Yield forecasting. *Agricultural Systems*, *40*(1), 211–236. https://doi.org/10.1016/0308-521X(92)90022-G

Huang, J., Wang, X., Li, X., Tian, H., & Pan, Z. (2013). Remotely sensed rice yield prediction using multi-temporal NDVI data derived from NOAA's-AVHRR. *PLoS ONE*, *8*(8), e70816. https://doi.org/10.1371/journal.pone.0070816

Huete, A. (1988). A soil-adjusted vegetation index (SAVI). *Remote Sensing of Environment*, *25*, 295–309. https://doi.org/10.1016/0034-4257(88)90106-x

Huete, A., Didan, K., Miura, T., Rodriguez, E. P., Gao, X., & Ferreira, L. G. (2002). Overview of the radiometric and biophysical performance of the MODIS vegetation indices. *Remote Sensing of Environment*, *83*(1), 195–213. https://doi.org/10.1016/S0034-4257(02)00096-2

Jackson, R. D., Idso, S. B., Reginato, R. J., & Pinter, Jr., P. J. (1981). Canopy temperature as a crop water stress indicator. *Water Resources Research*, *17*(4), 1133–1138. https://doi.org/10.1029/WR017i004p01133

Kayad, A. G., Al-Gaadi, K. A., Tola, E., Madugundu, R., Zeyada, A. M., & Kalaitzidis, C. (2016). Assessing the spatial variability of alfalfa yield using satellite imagery and ground-based data. *PLoS ONE*, *11*(6), e0157166. https://doi.org/10.1371/journal.pone.0157166

Kirkham, M. B., Johnson, D. E., Kanemasu, E. T., & Stone, L. R. (1983). Canopy temperature and growth of differentially irrigated alfalfa. *Agricultural Meteorology*, *29*(4), 235–246. https://doi.org/10.1016/0002-1571(83)90085-7

Lumley, T., & Miller, A. (2020). *Regression subset selection*. https://cran.r-project.org/web/packages/leaps/leaps.pdf

Major, D. J., Baret, F., & Guyot, G. (1990). A ratio vegetation index adjusted for soil brightness. *International Journal of Remote Sensing*, *11*(5), 727–740. https://doi.org/10.1080/01431169008955053

Merzlyak, M. N., Gitelson, A. A., Chivkunova, O. B., & Rakitin, V. Y. (1999). Non-destructive optical detection of pigment changes during leaf senescence and fruit ripening. *Physiologia Plantarum*, *106*(1), 135–141. https://doi.org/10.1034/j.1399-3054.1999.106119.x

Montandon, L. M., & Small, E. E. (2008). The impact of soil reflectance on the quantification of the green vegetation fraction from NDVI. *Remote Sensing of Environment*, *112*(4), 1835–1845. https://doi.org/10.1016/j.rse.2007.09.007

Montazar, A., Bachie, O., Corwin, D., & Putnam, D. (2020). Feasibility of moderate deficit irrigation as a water conservation tool in California's low desert alfalfa. *Agronomy*, *10*(11), 1640. https://doi.org/10.3390/agronomy10111640

Noland, R. L., Wells, M. S., Coulter, J. A., Tiede, T., Baker, J. M., Martinson, K. L., & Sheaffer, C. C. (2018). Estimating alfalfa yield and nutritive value using remote sensing and air temperature. *Field Crops Research*, *222*, 189–196. https://doi.org/10.1016/j.fcr.2018.01.017

Penney, D. C., Nolan, S. C., McKenzie, R. C., Goddard, T. W., & Kryzanowski, L. (1996). Yield and nutrient mapping for site specific fertilizer management. *Communications in Soil Science and Plant Analysis*, *27*(5-8), 1265–1279. https://doi.org/10.1080/00103629609369631

Penuelas, J., Baret, F., & Filella, I. (1995). Semi-empirical indices to assess carotenoids/chlorophyll a ratio from leaf spectral reflectance. *Photosynthetica*, *31*(2), 221–230.

Rashid, M., Bari, B. S., Yusup, Y., Kamaruddin, M. A., & Khan, N. (2021). A comprehensive review of crop yield prediction using machine learning approaches with special emphasis on palm oil yield prediction. *IEEE Access*, *9*, 63406–63439. https://doi.org/10.1109/ACCESS.2021.3075159

Robust regression: R data analysis samples. (n.d.). UCLA Statistical Computing Group. https://stats.idre.ucla.edu/r/dae/robust-regression/

Rondeaux, G., Steven, M., & Baret, F. (1996). Optimization of soil-adjusted vegetation indices. *Remote Sensing of Environment*, *55*(2), 95–107. https://doi.org/10.1016/0034-4257(95)00186-7

Rouse, J., Haas, R., Schell, J., & Deering, D. (1973, December). Monitoring vegetation systems in the great plains with ERTS. In *Proceedings of the Third Earth Resources Technology Satellite—1 Symposium*, Washington, DC. NASA.

Royo, C., Aparicio, N., Villegas, D., Casadesus, J., Monneveux, P., & Araus, J. L. (2003). Usefulness of spectral reflectance indices as durum wheat yield predictors under contrasting Mediterranean conditions. *International Journal of Remote Sensing*, *24*(22), 4403–4419. https://doi.org/10.1080/0143116031000150059

Sapkota, A., Meccage, E., Stougaard, R. N., Bicego, B., & Torrion, J. A. (2019). Applied boron increases alfalfa petiole boron concentration across water regimes, not yield. *Agronomy Journal*, *111*(6), 3220–3229. https://doi.org/10.2134/agronj2019.02.0085

Schwalbert, R. A., Amado, T. J. C., Nieto, L., Varela, S., Corassa, G. M., Horbe, T. A. N., Rice, C. W., Peralta, N. R., & Ciampitti, I. A. (2018). Forecasting maize yield at field scale based on high-resolution satellite imagery. *Biosystems Engineering*, *171*, 179–192. https://doi.org/10.1016/j.biosystemseng.2018.04.020

Segarra, J., González-Torralba, J., Aranjuelo, Í., Araus, J. L., & Kefauver, S. C. (2020). Estimating wheat grain yield using sentinel-2 imagery and exploring topographic features and rainfall effects on wheat performance in Navarre, Spain. *Remote Sensing*, *12*(14), 2278. https://doi.org/10.3390/rs12142278

Shen, M., Chen, J., Zhu, X., Tang, Y., & Chen, X. (2010). Do flowers affect biomass estimate accuracy from NDVI and EVI? *International Journal of Remote Sensing*, *31*(8), 2139–2149. https://doi.org/10.1080/01431160903578812

USDA-NASS. (2020). Crop production 2019 summary. *United States Department of Agriculture National Agricultureal Statistis Service*. https://www.nass.usda.gov/Publications/Todays_Reports/reports/cropan20.pdf

Xue, J., & Su, B. (2017). Significant remote sensing vegetation indices: A review of developments and applications. *Journal of Sensors*, *2017*, 1353691. https://doi.org/10.1155/2017/1353691

Zhang, L., Niu, Y., Zhang, H., Han, W., Li, G., Tang, J., & Peng, X. (2019). Maize canopy temperature extracted from UAV thermal and RGB imagery and its application in water stress monitoring. *Frontiers in Plant Science*, *10*. https://doi.org/10.3389/fpls.2019.01270

Zhang, P.-P., Zhou, X.-X., Wang, Z.-X., Mao, W., Li, W.-X., Yun, F., Guo, W.-S., & Tan, C.-W. (2020). Using HJ-CCD image and PLS algorithm to estimate the yield of field-grown winter wheat. *Scientific Reports*, *10*(1), 5173. https://doi.org/10.1038/s41598-020-62125-5

Zhang, Z., Liu, M., Liu, X., & Zhou, G. (2018). A new vegetation index based on multitemporal Sentinel-2 images for discriminating heavy metal stress levels in rice. *Sensors*, *18*(7), 2172. https://doi.org/10.3390/s18072172

How to cite this article: Sapkota, A., Haghverdi, A., & Montazar, A. (2023). Estimating fall-harvested alfalfa (*Medicago sativa* L.) yield using unmanned aerial vehicle–based multispectral and thermal images in southern California. *Agrosystems, Geosciences & Environment*, *6,* e20392. https://doi.org/10.1002/agg2.20392